Using Aerial Hyperspectral Remote Sensing Imagery to Estimate Corn Plant Stand Density

K. R. Thorp, B. L. Steward, A. L. Kaleita, W. D. Batchelor

Abstract. *Since corn plant stand density is important for optimizing crop yield, several researchers have recently developed ground-based systems for automatic measurement of this crop growth parameter. Our objective was to use data from such a system to assess the potential for estimation of corn plant stand density using remote sensing images. Aerial hyperspectral remote sensing imagery was collected on three dates over three plots of corn in central Iowa during the 2004 growing season. The imagery had a spatial resolution of 1 m and a spectral resolution of 3 nm between 498 nm and 855 nm. A machine vision system for early-season measurement of corn plant stand density was also used to map every row of corn within the three plots, and a complete inventory of corn plants was generated as a rich ground reference dataset. A principal component regression analysis was used to assess relationships between plant stand density measurements and principal components of hyperspectral reflectance for each plot, on each image collection date, and at three different spatial resolutions (2, 6, and 10 m). The maximum R^2 for regressions was 0.79. Estimates of corn plant stand density were best when using imagery collected at the later vegetative and early reproductive corn growth stages. Quantization effects due to row width complicated corn plant stand density estimates at 2 m spatial resolution, and better estimations were typically seen at resolutions of 6 m and 10 m. Among the different cases of plot, image date, and spatial resolution, the principal components of reflectance most highly correlated with plant stand density were able to be classified into four distinct types, denoted as types A, B, C, and D. Type A principal components contrasted all available visible red wavelengths with all available near-infrared wavelengths. Type B principal components contrasted green wavelengths (531 to 552 nm) plus shorter wave near-infrared (759 nm) with red wavelengths (675 to 693 nm) plus longer wave near-infrared (852 nm). Type C principal components summed green wavelengths (528 to 546 nm) and near-infrared wavelengths (717 to 855 nm). Type D principal components contrasted blue/green wavelengths (498 to 507 nm) with the red edge (717 nm). Remote sensing can be best used to estimate corn plant stand density at mid-season as long as plant stand variability exists and variability due to other factors is minimal.*

Keywords. *Corn, Hyperspectral, Machine vision, Population, Remote sensing, Spatial variability, Stand density.*

Plant stand density, or plant population, is an important crop growth parameter that influences corn (*Zea mays* L.) yield. Duncan (1958, 1984) determined that the weight of grain produced by individual corn plants decreases as the plant population increases, because at higher stand densities neighboring corn plants must compete more fiercely for resources. On the other hand, once corn plant population decreases beyond the level at which population pressure limits yield, the average yield per plant cannot continue to increase because plant genetics limit the weight of grain that a single plant can produce. Thus, for a given set of environmental conditions, there exists an optimum corn plant stand density at which corn yield will be maximized. Furthermore, due to the development and usage of corn hybrids that yield more at higher plant densities, recommended optimum planting densities have increased since the 1960s (Duvick and Cassman, 1999).

Spatial variability in corn plant population arises as a result of planter performance issues (Nielsen, 1995), emergence delays or failure (Nielsen, 1991), and early-season plant death due to stress. When these problems occur, the distribution of corn plants within the crop row, or the plant spacing, also becomes spatially variable across the field. The effect of interplant spacing variability on corn yield is unclear. Several studies have shown that corn yield decreased on the order of 159 kg ha^{-1} (3 bu acre^{-1}) for each 2.54 cm (1 in.) increase in the standard deviation of plant spacing (Krall et al., 1977; Nielsen, 1991). Nafziger (1996) found that corn plants growing on either side of a "skip" compensated for only 47% of the missing plant's grain at 44,479 plants ha^{-1} (18,000 plants acre^{-1}) and 19% of the missing plant's yield at 74,131 plants ha^{-1} (30,000 plants acre^{-1}), thus reducing overall crop yield. Although the yield of each plant in a "double" was 10% to 17% less than uniformly spaced plants, the net effect of doubles was to increase yield at all populations. Because both skips and doubles increased plant spacing variability but had opposite effects on yield, the researchers concluded that the skips and doubles affected yield mainly

Submitted for review in May 2006 as manuscript number IET 6484; approved for publication by the Information & Electrical Technologies Division of ASABE in October 2007. Presented at the 2006 ASABE Annual Meeting as Paper No. 063015.

The authors are **Kelly R. Thorp, ASABE Member Engineer,** Research Agricultural Engineer, USDA-ARS U.S. Arid-Land Agricultural Research Center, Maricopa, Arizona; **Brian L. Steward, ASABE Member Engineer,** Associate Professor, and **Amy L. Kaleita, ASABE Member Engineer,** Assistant Professor, Department of Agricultural and Biosystems Engineering, Iowa State University, Ames, Iowa; and **William David Batchelor, ASABE Member Engineer,** Professor and Department Head, Department of Agricultural and Biological Engineering, Mississippi State University, Mississippi State, Mississippi. **Corresponding author:** Kelly R. Thorp, USDA-ARS USALARC, 21881 N Cardon Ln., Maricopa, AZ 85238; phone: 520-316-6375; fax: 520-316-6330; e-mail: Kelly.Thorp@ars.usda.gov.

through changes in plant stand density. Vanderlip et al. (1988) found that plant spacing variability accounted for 5% to 23% of grain yield variability, and Liu et al. (2004) found no significant relationship between these two variables. Barbieri et al. (2000) planted corn in 0.35 m rows, one-half the conventional width, and increased plant spacing to maintain a plant population consistent with conventional methods. They found the narrow rows to increase grain yield by 27% to 46% under the condition of low nitrogen availability. Other experiments have shown that the use of narrow rows at higher than recommended plant populations can also significantly increase grain yield (Hunter et al., 1970; Porter et al., 1997; Widdicombe and Thelen, 2002). Although the effect of plant spacing variability on grain yield is unclear, results clearly show that row width modifications have potential to increase yield. Therefore, it can be concluded that, in addition to the total population, the distribution of plants over an area is also important for optimizing yield.

Since corn plant population has been known to have significant effects on grain yield, this crop growth parameter has been a topic of precision agriculture research. In terms of management, variable-rate seeding has been marketed to producers as a means to optimize yield spatially across the field. However, Bullock et al. (1998) cautions that this practice may not be economically beneficial for producers until more extensive information on the spatial relationship between plant population and crop yield is obtained for their fields. Other researchers have developed sensing technology for corn plant population and plant spacing variability measurement. Birrell and Sudduth (1995) mapped corn population at harvest with a mechanical sensor mounted on the corn header of a grain combine. Plant populations measured by the sensor were within 5% of plant population measured manually. Plattner and Hummel (1996) developed an optical sensor to map corn population at harvest, and the sensor was able to estimate average plant spacing with an error of 6.2%. Using a machine vision approach, Shrestha and Steward (2003) developed a sensing system for measurement of corn plant population and plant spacing in early growth stage corn. The sensing system utilized a video camera and a global positioning system (GPS) receiver to collect and locate image frames along corn rows, and video processing algorithms were developed for sequencing consecutive image frames, segmenting corn plants from soil background, and determining the geographic position of each corn plant in the row. System plant counts and manual plant counts were correlated with an r^2 of 0.90. Further developments in this work include a chain code methodology for delineating plant boundaries in sequenced video frames (Shrestha and Steward, 2005) and a statistical approach for improving the robustness of video processing algorithms over a wider range of field conditions (Shrestha et al., 2004a).

In addition to ground-based systems, aerial and satellite imaging systems have been regularly used to monitor the status of crop growth, and researchers have related spectral reflectance information obtained from these systems to crop growth parameters such as emergence date (Wanjura et al., 2003), percent canopy cover (Maas, 1998; Thorp et al., 2004), biomass development (Thenkabail et al., 2000), leaf area index (Bouman, 1992), and yield (GopalaPillai and Tian, 1999). However, there were no studies found in the literature in which remote sensing was used to estimate spatial variability in corn plant stand density. Our main objective in this work was therefore to relate the reflectance spectra from aerial hyperspectral remote sensing imagery to machine-vision-based measurements of corn plant stand density in an Iowa cornfield. Results of a principal component regression analysis were used to identify important spectral ranges and to determine the spatial and temporal limitations of using remote sensing for this purpose.

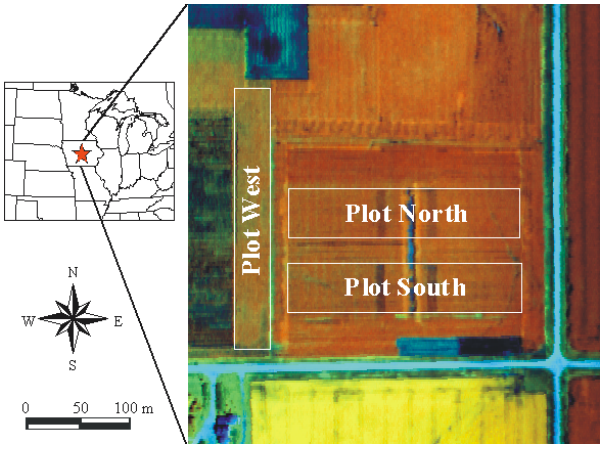

Figure 1. Data collection occurred over three sections of a cornfield in Iowa. Plots were arranged as shown on this 1 m spatial resolution image collected 25 July 2004.

Materials and Methods

Data Collection

Data collection occurred over three sections of a cornfield at Iowa State University's Agronomy and Agricultural Engineering Research Center west of Ames, Iowa (93.77879° W, 42.00988° N). The three data collection regions are aptly named Plot North (PN), Plot South (PS), and Plot West (PW) and are arranged as shown in figure 1. Each plot was approximately 1 ha in land area (table 1). On 4 June 2004, corn was planted in 76.2 cm (30 in.) rows in PN and PS. The planting of PN and PS was coordinated as part of another research project investigating the effects of planter speed, planter row unit design, and compaction on corn population and yield. These various treatments in addition to manual thinning in–

Table 1. Summary of important characteristics for the three data collection regions.

	Plot North	Plot South	Plot West
Land area	1.1 ha	1.1 ha	0.9 ha
Tillage	Conventional	No-till	Conventional
Planting date	4 June 2004	4 June 2004	13 June 2004
Planned variation[a]	Yes	Yes	No
GRDC[b] date	23 June 2004	23 June 2004	30 June 2004
RSIC[c] date 1	22 June 2004	22 June 2004	22 June 2004
RSIC date 2	25 July 2004	25 July 2004	25 July 2004
RSIC date 3	3 Sept. 2004	3 Sept. 2004	3 Sept. 2004
Cell count[d] (2 m)	2,576	2,599	2,159
Cell count (6 m)	259	259	210
Cell count (10 m)	88	88	75

[a] Variability in plant stand density was purposefully introduced.
[b] GRDC = ground reference data collection.
[c] RSIC = remote sensing image collection.
[d] Number of raster cells analyzed at the given spatial resolution.

creased the spatial variability of corn plant population within PS and PN. A conventional planting methodology was used to sow PW on 13 June 2004 (table 1).

Aerial hyperspectral remote sensing imagery was collected over the study area using the hyperspectral focal plane scanner and data acquisition system developed by scientists at the Institute for Technology Development at Stennis Space Center in Mississippi (Mao, 2000). A Cessna single-engine aircraft was used as the platform for remote sensing data collection, and the sensor was fastened in a gyrostabilized mount to minimize the effect of airplane roll, pitch, and yaw on data quality. The scanner collected data between 498 nm and 855 nm at a 3 nm bandwidth, for a total of 120 bands of spectral information. The spatial resolution of the imagery was 1 m. Remote sensing data were collected over the entire study area on three dates in the summer of 2004: 22 June, 25 July, and 3 September. These dates corresponded to corn growth stages V5 (5-leaf vegetative), V15 (15-leaf vegetative), and R4 (dough) for PN and PS, and V3 (3-leaf vegetative), V12 (12-leaf vegetative), and R2 (blister) for PW (table 2). Prior to remote sensing data collection, calibration tarps showing eight grayscale levels from white to black were laid out in an area near the study site. A spectroradiometer (1500, GER Corp., Millbrook, N.Y.) was used to measure the spectral reflectance from each panel between 286 nm and 1102 nm at a bandwidth of approximately 1.5 nm. Pilots then captured hyperspectral remote sensing imagery over both the study area and over the calibration tarps.

Ground reference data were collected using the machine vision-based corn plant population sensing system developed by Shrestha and Steward (2003). System components were mounted on a 4×4 Kawasaki all-terrain vehicle (ATV) for data collection in the field (fig. 2). A digital camcorder (DCR-TRV900, Sony Corp., New York, N.Y.) was used for video acquisition of crop rows, and a special mount was designed to hold the camera at the front center of the vehicle. Special features of the camera mount included a metal frame skirted with translucent white cloth for diffusion of sunlight in the camera's field of view and a connection mechanism that isolated the camera from vehicle vibrations. The camera was mounted at a height of 0.53 m above the ground, and this provided a 0.3 × 0.4 m field of view. Video of crop rows was recorded onto miniDV tapes. A global positioning system (GPS) receiver (GG24-RTK, Thales Navigation, Santa Clara, Cal.) was used to obtain the geographic coordinates of the ATV in the field. The antenna for the GPS receiver was mounted above the storage box at the rear center of the vehicle, and the distance between the video camera and the receiver along the longitudinal axis of the vehicle was 1.73 m. A GPS encoder/decoder (VMS 200, Red Hen Systems, Inc., Fort Collins, Colo.) was used to convert GPS strings to an audio signal that could be recorded on the soundtrack of the miniDV tapes. A corrugated aluminum storage box was mounted on the rear of the ATV for storage of the global positioning equipment.

Table 2. Status of corn growth on each image collection date.[a]

	Plot North		Plot South		Plot West	
Image Date	DAP	GS	DAP	GS	DAP	GS
22 June 2004	18	V5	18	V5	9	V3
25 July 2004	51	V15	51	V15	42	V12
3 Sept. 2004	91	R4	91	R4	82	R2

[a] DAP = days after planting; GS = growth stage.

Figure 2. The ground-based corn plant population sensing system.

On the days of ground reference data collection at the study site, a second GPS receiver (GG24-RTK, Thales Navigation, Santa Clara, Cal.) was placed at the location of a benchmark on the research farm. This receiver was used as a base station to improve the accuracy of position measurements at the rover receiver on the ATV. The two GPS receivers communicated with each other via a radio link (RFM-96W, Pacific Crest Corp., Santa Clara, Cal.). When the rover receiver was fixed on the base station through the radio link, the positioning accuracy of the rover receiver was less than 10 cm. The video camera was then set to collect video in progressive scan mode with a shutter speed of 1/1000 s. Due to the movement of the ATV, these settings were essential to ensure that high-quality video was collected. After fully zooming out the camera and allowing it to automatically focus on the scene, the camera's autofocus function was turned off. If left on, the autofocus was found to continually overcompensate as it attempted to adjust the camera's focus during data collection, and this ultimately caused blurriness in the video. Prior to video collection, the camera's white balance was also adjusted to ensure a more natural video color. All other camera controls were used at their default settings. Video frames recorded onto the miniDV tapes were in the NTSC DV format with an aspect ratio of 2:3 (480 × 720 pixels) and 24-bit color resolution. Frames recorded in this format do not have square pixels but are stretched to cover the camera's field of view, having an aspect ratio of 3:4. Different aspect ratios between real-world and recorded frames do not affect image processing; this difference only affects the display of the image frames on computer screens with square pixels. The GPS information was recorded on the soundtrack at a frequency of 5 Hz, and the ATV was operated at an average speed of 1 m s^{-1}. Ground reference data were collected in PN and PS on 23 June 2004 and in PW on 30 June 2004 (table 1). The system was used to collect information over every crop row contained within the area of the three plots.

Ground Reference Data Processing

Following the initial development of their machine vision system, Shrestha and Steward (2003) packaged their algorithms for system operation and video processing into a C++

application named ESCOPE. Characteristics of the software include two operation modes, including "real-time mode" for automatic collection of corn plant population and spacing information in the field and "laboratory mode" for analysis of pre-recorded videotapes in the laboratory. The ESCOPE software also provides three options for image segmentation, including a new algorithm that significantly reduces the processing time required for this task (Shrestha et al., 2004b). In addition, a manual plant count adjustment algorithm and graphic user interface were developed such that a user could visually inspect and make corrections to the automatic plant counting algorithm results on the computer screen. Due to the difficulties in automatically delineating plants at higher growth stages, such corrections were most needed when attempting to count larger plants.

To generate a ground reference dataset of corn plant population for this work, the ESCOPE software first was used in laboratory mode to segment the video frames that were recorded during the data collection effort. To save time, the fast image segmentation algorithm (Shrestha et al., 2004b) was used as a first choice. However, when poor field conditions or video quality warranted a more robust algorithm, the slower algorithm presented in Shrestha and Steward (2003) was used. Plant identification and counting were then performed on all the sequenced images of crop rows using an image segmentation algorithm (Shrestha and Steward, 2003) combined with a chain code approach (Shrestha and Steward, 2005). However, because crop rows were mainly recorded at higher growth stages in this work, manual adjustments were made in a majority of the sequenced images to ensure the accuracy of plant locations. After these adjustments, ESCOPE produced a text file containing the geographic coordinates of all marked plants in the sequenced images. Because video was recorded and analyzed on every crop row, the ground-based system was used to generate a complete inventory of all corn plant locations within our study area. The generation of this dataset was quite costly in terms of manual effort; however, it enabled a unique investigation into the use of remote sensing imagery as an alternative way to estimate plant population spatially across cornfields.

Hyperspectral Data Processing

The hyperspectral imagery was prepared for analysis using both spatial and spectral preprocessing. First, since raw image spatial distortions can be produced by changes in aircraft attitude during the scanner-based image collection process, a correction procedure, developed by Yao and Tian (2004), was implemented to remove as much spatial distortion in the raw hyperspectral imagery as possible. Next, the images were georeferenced to the Universal Transverse Mercator (UTM) coordinate system using a field boundary map that was obtained with a meter-level accuracy backpack GPS unit (Pathfinder Pro XRS, Trimble Navigation Ltd., Sunnyvale, Cal.). For spectral correction, a minimum noise fraction (MNF) transformation (Green et al., 1988) was used to remove sensor noise in the raw reflectance data. Then, by matching the digital numbers of the calibration tarps in each image to the reflectance measurements taken of the tarps on the ground, the imagery was calibrated to percent reflectance with an empirical line calibration procedure (Smith and Milton, 1999). These pre-processing steps were performed separately for each of the three remote sensing image collection dates using ENVI software (Version 4.2, Research Systems, Inc., Boulder, Colo.).

Statistical Analysis

In preparation for statistical analysis, ground reference data and spectral reflectance data were aggregated at three separate spatial resolutions. Since all the remote sensing images were originally collected at 1 m spatial resolution, the reflectance measurements in each waveband were averaged over square blocks of 4, 36, and 100 raster units to decrease the spatial resolution of the imagery arbitrarily to 2 m, 6 m, and 10 m, respectively. The total number of grid cells for PN, PS, and PW resulting from this aggregation process are given in table 1. Using ArcGIS (Version 9, ESRI, Redlands, Cal.), the raster grids for images on each date and at each spatial resolution were then used to clip the ground reference corn population measurements over each of the three plots. The total number of plants within each raster grid cell area was then determined, and the plant counts were normalized by the grid cell area to generate raster maps of corn plant stand density. Since corn population was measured on the ground only once during the season, we assumed that the plant stand was well established at the time of the ground-based measurements and that the corn population did not change significantly throughout the remainder of the growing season.

For purposes of data reduction and interpretation, principal component analyses (Johnson and Wichern, 2002) were performed separately on the hyperspectral reflectance data for each combination of plot, measurement date, and spatial resolution. A principal component analysis requires the computation of the singular value decomposition of a dataset. It results in an orthogonal linear transformation of the dataset such that the first coordinate axis lies along the vector of maximum variability in the dataset, and each succeeding coordinate axis lies along the vector of maximum variability in a direction orthogonal to the preceding axes. For this study, if $\mathbf{X}$ is the $m \times n$ matrix of hyperspectral reflectance information, where m is the number of wavebands and n is the number of grid cells across a plot, then the m principal components for the dataset are ordered in the $m \times n$ matrix, $\mathbf{Y}$, such that:

$$\mathbf{Y} = \mathbf{U}^T \mathbf{X} = \Sigma \mathbf{V}^T \quad (1)$$

where $\mathbf{U}\,\Sigma\,\mathbf{V}^T$ is the singular value decomposition of $\mathbf{X}$. The results of a principal component analysis are often discussed in terms of the scores (rows of $\mathbf{Y}$) and the loadings (columns of $\mathbf{U}$). Principal component loadings are otherwise known as the eigenvectors of the covariance matrix of $\mathbf{X}$, and the eigenvalues of the covariance matrix of $\mathbf{X}$ are contained in the diagonal elements of Σ. In the case where an $m \times n$ matrix, $\mathbf{Z}$, containing the standardized variables of $\mathbf{X}$ is used in place of $\mathbf{X}$ in equation 1, the principal component loadings are the eigenvectors of the correlation matrix of $\mathbf{X}$. All reflectance information was standardized prior to computing the principal components in this study.

The principal component scores for each case of plot, measurement date, and spatial resolution were used as the predictor variables in a multiple linear regression analysis (Neter et al., 1996) with corn plant stand density as the response variable. Unique regression models were fit for each case using the first k principal component scores as predictor variables, iterating k from 0 to 12. Regression models for each case were evaluated using leave-one-out cross-

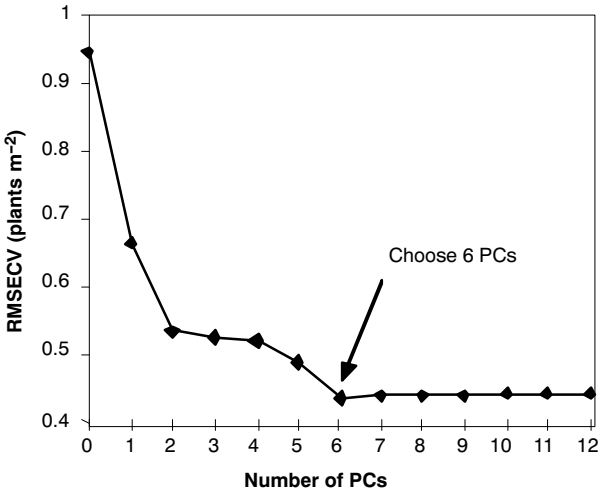

Figure 3. Scree plot for Plot North at 6 m spatial resolution for the 25 July image.

validation, and our reported values for the coefficient of multiple determination (R^2) and the root mean squared error of cross-validation (RMSECV) are the cross-validated estimates of regression model performance. Scree plots (RMSECV versus *k*) were used to determine the appropriate number of principal components to be included in the reported regression results. This endeavor was somewhat subjective; we chose the number of principal components at the local minimum on the scree plot after which the RMSECV did not significantly change (fig. 3). Correlation coefficients (*r*) were also computed to assess the relationship between each principal component score and plant stand density. By examining the loadings for the principal components most highly correlated with stand density, we assessed how the original reflectance spectra contributed to the most important principal components. Algorithms for carrying out the principal component analyses, the regressions on principal component scores, the leave-one-out cross-validation procedure, and the analysis and interpretation of the results are all available in the "pls" package (Mevik and Wehrens, 2007) of the R statistical software.

Results

Principal Component Regression

Among the three spatial resolutions used in the analysis, the 2 m spatial resolution generally provided the poorest relationships between observed plant stand density and cross-validated estimates from multiple linear regressions on principal component scores (table 3). The R^2 values for these regressions ranged from 0.02 to 0.40 at the 2 m spatial resolution, and the RMSECVs ranged from 1.37 to 1.75 plants m^{-2}. The reason for poorer results at the 2 m spatial resolution can be explained in terms of the crop row width. In this study, crop rows were planted at a width of 0.76 m (30 in). Thus, depending on the location of the 2 m spatial resolution raster grid relative to the crop rows, some raster cells would contain three crop rows while adjacent cells would contain only two crop rows. If a raster cell contained three crop rows, the plant count for the cell would be significantly higher than for the cells containing only two crop rows. Given the low R^2 values and higher RMSECV values at 2 m spatial resolution, it is evident that this crop row quantization effect was unable to be detected within the remote sensing imagery. These results make sense, since light interaction within a plant canopy is not restricted to the bounds of a raster grid, whereas plant population can be discretely measured within that grid. At the 6 m and 10 m spatial resolutions, a greater number of crop rows were present within each raster grid cell, which reduced the effect of row quantization on plant counts in the cells. As a result, estimates of plant stand density were always improved for these lower spatial resolution cases.

Table 3. Cross-validated results for regressions of principal component (PC) scores and corn plant stand density for each case of plot, spatial resolution, and image collection date.

	Number of PCs[a]			R^2			RMSECV[b] (plants m^{-2})		
Date	2 m	6 m	10 m	2 m	6 m	10 m	2 m	6 m	10 m
Plot North									
22 June	6	3	4	0.31	0.55	0.52	1.45	0.61	0.39
25 July	2	6	6	0.38	0.79	0.70	1.37	0.44	0.30
3 Sept.	4	4	5	0.30	0.59	0.49	1.45	0.60	0.42
Plot South									
22 June	6	5	4	0.11	0.25	0.38	1.75	1.03	0.65
25 July	2	5	5	0.40	0.76	0.75	1.45	0.60	0.39
3 Sept.	4	5	5	0.37	0.74	0.63	1.46	0.60	0.49
Plot West									
22 June	7	7	7	0.02	0.25	0.34	1.55	0.46	0.33
25 July	4	2	7	0.15	0.36	0.45	1.42	0.40	0.29
3 Sept.	2	2	2	0.14	0.52	0.56	1.39	0.34	0.29

[a] Number of principal components used in the regression (chosen from scree plots).
[b] Root mean squared error of cross-validation.

When comparing the statistics across the three image collection dates, the relationships between observed corn plant stand density and cross-validated regression model estimates were better for the 25 July image for PN and PS (table 3). At the 6 m spatial resolution, the highest two R^2 values in the entire study (0.79 and 0.76 for PN and PS, respectively) were achieved when relating the principal components of reflectance spectra from 25 July to corn plant stand density (fig. 4). In addition, the RMSECVs for PN and PS on 25 July were generally lower than that on the other two dates. The only exception was for PS on 3 September at 6 m spatial resolution, which essentially had an identical RMSECV value as the estimate from 25 July. For PW, the best relationships between observed corn plant stand density and cross-validated model estimates generally occurred with data from the 3 September image, reflecting the later planting date for PW. Although the highest R^2 value for PW was only 0.56 on 3 September at the 10 m spatial resolution, the lowest RMSECV for the entire study, 0.29 plants ha^{-1}, was also achieved in this case. Thus, although the regression model explained a relatively lower percentage of overall variability for this case, the error between measured and estimated values was not excessive in relation to other cases.

Estimates of corn plant stand density were generally poorer when using the data from the 22 June image. On the 22 June image collection date, corn plants were still in their early vegetative growth stages (table 2), and canopy closure had not yet occurred. At early growth stages, the effects of soil background on reflectance spectra have been known to hamper the analysis of remote sensing imagery for vegetation (Thorp et al., 2004). Similarly in this study, results indicated

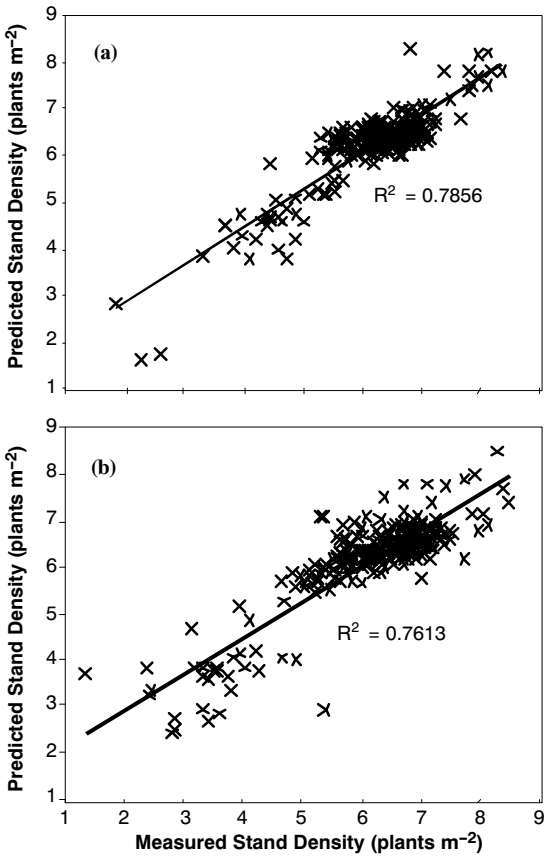

Figure 4. Measured plant stand density versus cross-validated estimates from principal component regression for (a) Plot North and (b) Plot South at 6 m spatial resolution on 25 July 2004.

that the use of remote sensing imagery to estimate the vegetative growth parameter of plant stand density was less reliable at earlier growth stages before the canopy had closed. We also expected to see a reduced ability to estimate corn plant stand density from reflectance spectra at the end of the growing season as the plants reached physiological maturity and lost vegetative vigor. Our results for PN and PS confirm this, since the R^2 values for the 3 September image were lower than that for the 25 July image. Likewise, with the exception of one case, the RMSECVs were always higher with the 3 September image than with the 25 July image for PN and PS. Plants in PN and PS were at the V15 and R4 growth stages on 25 July and 3 September, respectively (table 2). Plant population in PW was best estimated from the principal components of reflectance spectra on 3 September when plants were at the R2 growth stage. Thus, remote sensing imagery was best used to estimate the vegetative growth parameter of plant stand density when plants were at the upper vegetative and lower reproductive growth stages.

Other interesting results were found when comparing the regression statistics between the three plots for each collection date and spatial resolution. First, for the 22 June image collection date, the R^2 values for PN were higher than for PS and the RMSECVs for PN were lower than for PS at all three spatial resolutions. Prior to planting, PN was tilled using a conventional tillage method, while PS was managed using no-till practices (table 1). As a result, it is expected that the higher proportion of residue covering the surface of PS increased the soil brightness in that plot. Since increasing soil brightness has been shown to cause reduced correlations of reflectance spectra to vegetative growth parameters at early growth stages (Thorp et al., 2004), the residue cover in PS probably increased the difficulty in estimating corn plant stand density on the 22 June date relative to PN. Second, the R^2 values for PW were lower than that of PN and PS for most cases of image date and spatial resolution. It is expected that the total corn population variability across each plot contributed to this result. The standard deviations for corn plant density, aggregated at the 6 m spatial resolution, were 0.91, 1.20, and 0.53 plants m^{-2} for PN, PS, and PW, respectively. In addition, a histogram of the data showed that plant density ranged from 2 to 9 plants m^{-2} for PN and PS, but it only ranged from 6 to 9 plants m^{-2} for PW (fig. 5).

Lower R^2 values for PW in relation to PN and PS may be understood according to the definition of the statistic. The R^2 statistic is the percentage of total variability in a dataset that is explained by a regression model; it demonstrates the existence of a trend between the model estimates and measured data. Therefore, if a dataset has less overall variability to be explained, as is the case for PW, then the variability due to model error can approach the variability in the measured data, leaving little trend between the measured and estimated values. As a result, the R^2 statistic is reduced. It is interesting to note that, although R^2 values were typically lower for PW, the values for RMSECV in PW were also lower than that in PN and PS for many cases. However, unlike the R^2 statistic, the RMSECV statistic does not give an indication of a trend between the regression model estimates and the measured data. These results for PW are important in light of our objective; remote sensing imagery may only be useful for estimating plant stand variability if (1) stand variability exists and (2) the variability due to factors other than plant stand is minimal.

Principal Component Interpretation

Pearson correlations between plant stand density and each of the first seven principal component scores for each case demonstrated similar results as that obtained from principal component regression (table 4). When comparing the different spatial resolutions, the effect of row quantization was apparent, since the 6 m or 10 m resolution datasets typically had one or two principal component scores that were more highly correlated with plant stand density than that of the 2 m spatial resolution datasets. In addition, across all of the 22 June data–

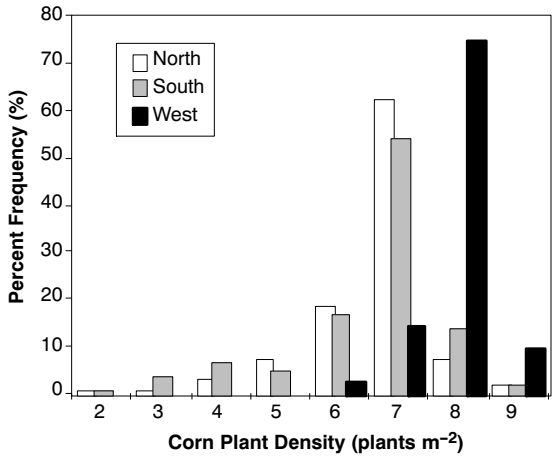

Figure 5. Histograms of corn plant stand density in each plot aggregated at 6 m spatial resolution.

Table 4. Pearson correlations between plant stand density and each of the first seven principal component (PC) scores for each case of plot, spatial resolution, and image collection date. Classifications (type A, B, C, or D) of the PCs were assigned when the correlation exceeded 0.25.

		North			South			West		
Date	PC	2 m	6 m	10 m	2 m	6 m	10 m	2 m	6 m	10 m
22 June	1	-0.07	-0.08	0.19	-0.04	-0.19	-0.14	0.03	-0.02	0.12
	2	**-0.46 A**	**0.56 A**	**0.31 A**	**-0.27 A**	**-0.40 A**	**-0.49 A**	-0.02	0.14	**0.29 D**
	3	-0.09	**0.50 B**	**0.61 B**	-0.15	0.21	**-0.31 B**	-0.07	0.05	-0.09
	4	**-0.25 B**	0.03	**0.26 D**	0.02	-0.04	**-0.31 D**	-0.03	0.19	-0.17
	5	0.08	0.07	-0.10	0.09	0.20	0.05	0.01	-0.01	0.03
	6	-0.13	0.08	0.09	-0.09	-0.04	0.10	-0.10	**-0.31 B**	**0.50 B**
	7	0.04	0.02	0.05	0.02	0.03	-0.05	-0.07	**-0.40 B**	**-0.30 B**
25 July	1	**-0.55 A**	**-0.72 A**	**0.48 A**	**-0.58 A**	**-0.75 A**	**0.61 A**	**-0.27 A**	**-0.44 A**	**-0.35 A**
	2	**-0.28 C**	**-0.42 C**	**-0.46 C**	**-0.26 C**	**-0.41 C**	**0.59 C**	-0.23	**-0.43 C**	**-0.52 C**
	3	-0.05	-0.11	-0.07	-0.01	-0.03	0.02	0.13	-0.06	-0.06
	4	-0.03	-0.10	**-0.31 B**	0.00	-0.02	0.02	0.08	-0.01	-0.20
	5	-0.04	-0.19	0.19	-0.04	0.21	**0.30 D**	0.04	0.10	0.09
	6	-0.07	-0.23	**0.43 D**	0.03	0.07	0.05	0.07	0.18	-0.20
	7	0.08	-0.02	-0.08	-0.09	-0.04	0.08	0.06	0.08	-0.24
3 Sept.	1	0.11	-0.17	-0.19	-0.08	0.03	-0.13	-0.19	**0.59 A**	**-0.61 A**
	2	**0.39 A**	**0.49 A**	**0.18 A**	**0.55 A**	**0.73 A**	**0.53 A**	**0.32 A**	**-0.44 C**	**-0.47 C**
	3	**-0.30 B**	**0.35 B**	0.04	-0.22	**-0.35 B**	**0.47 B**	0.00	0.08	0.03
	4	0.22	**-0.47 D**	**0.39 D**	-0.15	0.16	-0.02	0.01	-0.11	0.06
	5	0.02	-0.01	**-0.58 D**	0.07	**-0.27 D**	**0.41 D**	0.04	-0.02	0.01
	6	-0.02	0.08	0.02	-0.02	-0.15	0.05	0.02	0.01	0.05
	7	0.12	-0.22	0.00	-0.14	0.16	0.24	0.06	0.07	0.23

sets, the first principal component was never the most highly correlated with plant stand density. This indicated that the information along the axis of greatest variability in the datasets were due to something other than plant stand density, probably soil background. On the other hand, across all of the 25 July datasets, the first two principal components were always the most highly correlated with plant stand density. This indicated that the information along the first two orthogonal axes of greatest variability in the datasets was highly related to plant stand density. However, by 3 September, the first principal component for each PN and PS dataset was no longer the most highly related to plant stand density. This is not true for PW, which was planted later than PN and PS. These results further support that idea that information in remote sensing images was best able to estimate corn plant stand density at mid-season when the corn was at the late vegetative to early reproductive growth stages. For PW on 22 June, the sixth and seventh principal components were most highly correlated with stand density, indicating the relatively small effect of vegetation in this reflectance data.

Principal component loadings can be thought of as weighting values per wavelength in the transformation of reflectance data to the principal component scores (eq. 1). By visually comparing the loading plots of principal components whose correlations with plant stand density were greater than the arbitrarily chosen value of 0.25 (table 4), we were able to classify the most important principal components for estimating plant stand density and to interpret the relationship between each component type and the original reflectance data. Four unique types of principal components, labeled as types A, B, C, and D in table 4, were identified. Examples of the loading plots for each principal component type are given in figure 6, where the presented loading plot for each type corresponds to the principal component of that type, among all cases, that had the highest correlation between principal component scores and plant stand density. For example, with r equal to –0.75, the most highly correlated type A principal component was the first principal component of the dataset for PS on 25 July at the 6 m spatial resolution (table 4).

The type A principal component represents a contrast between reflectance measurements in the visible red and near-infrared regions of the electromagnetic spectrum. For the case shown in figure 6 (PS, 25 July, 6 m spatial resolution, first component), wavelengths in the visible red range were given a strong positive loading while wavelengths in the near-infrared had a strong negative loading. Therefore, as near-infrared reflectance increased and visible red reflectance decreased with increasing plant stand density, the principal component score would be reduced. This resulted in a negative correlation (–0.75) between principal component scores and plant stand density for this case (table 4). In other

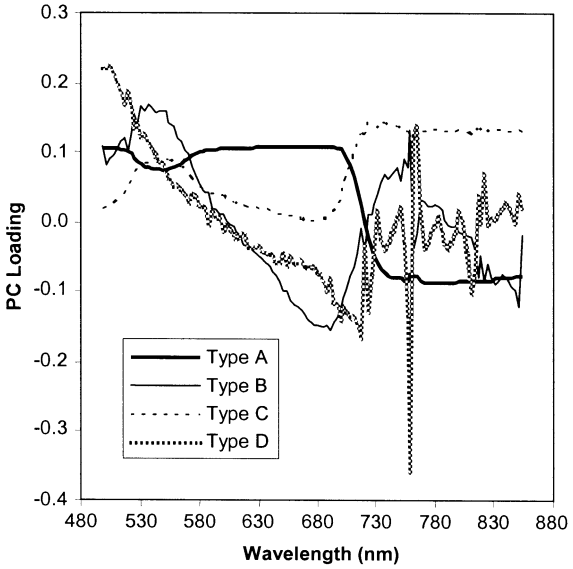

Figure 6. Loading values for four common principal component (PC) types that were highly correlated to plant stand density.

cases, the wavelengths in the visible red range had a negative loading and wavelengths in the near-infrared had a positive loading, which resulted in positive correlations between principal component scores and plant stand density. The inflection point of zero loading for type A principal components occurred between 717 and 720 nm. This approximately corresponds to the location of the red edge (Horler et al., 1983), which is the transition point between absorption of visible red light and reflection of near-infrared light in plant leaves. By contrasting the reflectance in these portions of the spectrum, the type A principal component is an indicator of the amount of vegetation available for reducing reflectance in the visible red region, increasing reflectance in the near-infrared region, and increasing the overall spread between the amount of visible and near-infrared light reflected from the plant canopy. In nearly all the cases, the type A component was the primary principal component of those that were highly correlated to plant stand density (table 4). Therefore, of the variability in reflectance data that was due to vegetation, the largest portion was related to the opposing effect of plant leaves on reflectance of light in the visible red and near-infrared regions.

The type B principal component represents a contrast between reflectance measurements in the green and red portions of the spectrum as well as a second contrast between two portions of the near-infrared region. For the case shown in figure 6 (PN, 22 June, 10 m spatial resolution, third component), a range of wavelengths in the green region from 531 to 552 nm had a strong positive loading while a range of wavelengths in the red region from 675 to 693 nm had strong negative loading. In addition, the loading in the near-infrared at 759 nm was strongly positive while the near-infrared loading at 852 nm was strongly negative. If plant stand density was very small and reflectance spectra were dominated by the soil signal, then we would expect the reflectance in the red wavelengths to exceed the reflectance in the green wavelengths. Likewise, we would expect the reflectance at 852 nm in the near-infrared region to exceed the reflectance at 759 nm. With given loadings for the type B principal component, this would result in principal component scores that were more negative in value. However, with an increase in plant stand density, we would expect an increase in green reflectance and a decrease in red reflectance, and the green reflectance would eventually exceed that of the red. Likewise, we would expect the reflectance in the near-infrared to level off, and the contrast of reflectance between 759 and 852 nm would zero out. This would result in principal component scores that were more positive in value. Thus, there exists a positive correlation (0.61) between principal component scores and plant stand density for this case (table 4). Interestingly, in PN and PS, the type B principal component is the most common secondary component for cases on 22 June and 3 September, dates when partial canopy cover or onset of plant senescence reduced the influence of vegetation on the reflectance spectra. Thus, the type B principal component is important for plant stand density estimation when the reflectance spectra are dominated by components other than vegetation.

The type C principal component sums the reflectance in the green region with the reflectance in the near-infrared region. For the case shown in figure 6 (PS, 25 July, 10 m spatial resolution, second component), strong positive loadings were computed in the green region from 528 to 546 nm and in the near-infrared region from the red edge at 717 nm through the longest measured wavelength of 855 nm. Loading values in the red region are essentially zero. Thus, the scores for this component are directly related to the increases in green and near-infrared reflectance that would be expected with increases in plant stand density, and there is a positive correlation (0.59) between principal component scores and plant stand density for this case (table 4). The type C principal component is similar to the type B component in that it was usually a secondary component to type A; however, type C was most commonly found on 25 July and 3 September for PW when the vegetation signal was more dominant in the remote sensing data.

The type D principal component represents a contrast between the shorter green wavelengths and the red edge. For the case shown in figure 6 (PN, 3 September, 10 m spatial resolution, fifth component), strong positive loadings were computed between the blue and green regions from 498 to 507 nm, and the loadings gradually declined to a strong negative loading at the red edge wavelength of 717 nm. Loadings in the near-infrared are noisy around zero, contributing nothing to the contrast, and the negative spike at 759 nm is more than likely related to the Fraunhofer line at that wavelength. With increasing plant stand density, reflectance in the blue to short green region is expected to decline due to absorption by chlorophyll while reflectance at the red edge increases. Therefore, this contrast produces principal component scores that become more negative as plant stand density increases, and we obtain a negative correlation (–0.58) between principal component scores and plant stand density for this case. It is interesting to note that the important wavelengths in the green region for this component approached the spectral limits of the remote sensing system, and it would be interesting to understand how this component would behave if reflectance data were available at wavelengths less than 498 nm.

DISCUSSION

Remote sensing technology was shown to be effective at estimating corn plant stand density at mid-season. This work fills a research gap in the area of corn population sensing, which to date has only been developed for counting plants during the early stages of corn growth (Shrestha and Steward, 2003) and while harvesting (Birrell and Sudduth, 1995). Effective use of remote sensing imagery for estimating population was shown to depend heavily on timing. Therefore, for efforts to be fruitful, plans for data reconnaissance must be well executed to acquire imagery when corn plants are reaching the later vegetative growth stages. If image collection dates are too early, results may be hampered by the strong influence of soil background on reflectance spectra. If remote sensing images are collected too late in the growing season, the onset of reproductive development and senescence prevents the use of reflectance spectra for estimating plant population.

The characteristics of the ground reference dataset in this work demonstrate the usefulness of ground-based crop sensing systems for testing the effectiveness of remote sensing technology. Since the entire area of each plot was mapped for corn plant geographic locations, no assumptions were made regarding corn population in unmeasured locations and there was no extrapolation of population measurements to larger areas based on strategic sampling. This was possible due to the existence of the ground-based corn population sensing

system developed by Shrestha and Steward (2003). Future research in agricultural remote sensing will benefit from the development of ground-based sensing systems that can relatively quickly generate maps of important crop growth and soil parameters across the field. By first acquiring a detailed map of these parameters on the ground, a truer assessment of the limitations of remote sensing can be obtained as camera systems are incorporated on aerial and satellite platforms farther away from the scene. Then, it is possible to determine whether remote sensing offers any advantages over ground-based data collection and whether remote sensing images can be used to accurately estimate the true variability of crop parameters on the ground. For example, this study showed that remote sensing offers an advantage over ground-based data collection at mid-season; however, corn plant stand density could not be estimated at higher spatial resolutions due the effects of row quantization within an image's raster grid.

Conclusions

- Remote sensing was best able to estimate corn plant stand density at mid-season when plants were at the late vegetative or early reproductive growth stages.
- Due to crop row quantization effects, poor relationships between principal components of reflectance and plant stand density were obtained for datasets at a 2 m spatial resolution. Improved relationships were found for datasets at 6 m and 10 m spatial resolutions.
- Remote sensing imagery may only be useful for estimating plant stand variability if stand variability exists and if the variability due to other factors is minimal.
- Principal components of reflectance that were most highly correlated with plant stand density were classified into four common types based on the loading values.

Acknowledgements

This research was supported by the Hatch Act and State of Iowa funds. The authors also express sincere thanks to the Institute of Technology Development in Urbana, Illinois, and NASA for collection of aerial hyperspectral remote sensing imagery and to Pioneer Hi-Bred International, Inc., in Johnston, Iowa, for use of their data collection equipment.

References

Barbieri, P. A., H. R. Sainz Rozas, F. H. Andrade, and H. E. Echeverria. 2000. Row spacing effects at different levels of nitrogen availability in maize. *Agron. J.* 92(2): 283-288.

Birrell, S. J., and K. A. Sudduth. 1995. Corn population sensor for precision farming. ASAE Paper No. 951334. St. Joseph, Mich.: ASAE.

Bouman, B. A. M. 1992. Accuracy of estimating the leaf area index from vegetation indices derived from crop reflectance characteristics, a simulation study. *Intl. J. Remote Sensing* 13(16): 3069-3084.

Bullock, D. G., D. S. Bullock, E. D. Nafziger, T. A. Doerge, S. R. Paszkiewicz, P. R. Carter, and T. A. Peterson. 1998. Does variable rate seeding of corn pay? *Agron. J.* 90(6): 830-836.

Duncan, W. G. 1958. The relationship between corn population and yield. *Agron. J.* 50: 82-84.

Duncan, W. G. 1984. A theory to explain the relationship between corn population and grain yield. *Crop Sci.* 24(6): 1141-1145.

Duvick, D. N., and K. G. Cassman. 1999. Post-green revolution in yield potential of temperate maize in the north-central United States. *Crop Sci.* 39(6): 1622-1630.

GopalaPillai, S., and L. Tian. 1999. In-field variability detection and spatial yield modeling for corn using digital aerial imaging. *Trans. ASAE* 42(6): 1911-1920.

Green, A. A., M. Berman, P. Switzer, and M. D. Craig. 1988. A transformation for ordering multispectral data in terms of image quality with implications for noise removal. *IEEE Trans. Geosci. and Remote Sensing* 26(1): 65-74.

Horler, D. N. H., M. Dockray, and J. Barber. 1983. The red edge of plant leaf reflectance. *Intl. J. Remote Sensing* 4(2): 273-288.

Hunter, R. B., L. W. Kannenberg, and E. E. Gamble. 1970. Performance of five maize hybrids in varying plant populations and row widths. *Agron. J.* 62(2): 255-256.

Johnson, R. A., and D. W. Wichern. 2002. *Applied Multivariate Statistical Analysis.* 5th ed. Patparganj, Delhi, India: Pearson Education.

Krall, J. M., H. A. Esechie, R. J. Raney, S. Clark, G. TenEyck, M. Lundquist, N. E. Humburg, L. S. Axthelm, A. D. Dayton, and R. L. Vanderlip. 1977. Influence on within-row variability in plant spacing on corn grain yield. *Agron. J.* 69(5): 797-799.

Liu, W., M. Tollenaar, G. Stewart, and W. Deen. 2004. Within-row plant spacing variability does not affect corn yield. *Agron. J.* 96(1): 275-280.

Maas, S. J. 1998. Estimating cotton canopy ground cover from remotely sensed scene reflectance. *Agron. J.* 90(3): 384-388.

Mao, C. 2000. Hyperspectral focal plane scanning: An innovative approach to airborne and laboratory pushbroom hyperspectral imaging. In *Proc. 2nd Intl. Conference on Geospatial Information in Agriculture and Forestry* 1: 424-428. Ann Arbor, Mich.: ERIM International.

Mevik, B., and R. Wehrens. 2007. The pls package: Principal component and partial least squares regression in R. *J. Stat. Software* 18(2). Available at: www.jstatsoft.org/v18/i02/v18i02.pdf.

Nafziger, E. D. 1996. Effects of missing two-plants hills on corn grain yield. *J. Prod. Agric.* 9(2): 238-240.

Neter, J., M. H. Kutner, C. J. Nachtsheim, and W. Wasserman. 1996. *Applied Linear Statistical Models.* Boston, Mass.: WCB McGraw-Hill.

Nielsen, R. L. 1991. Stand establishment uniformity in corn. AGRY-91-01. Purdue, Ind.: Purdue University, Department of Agronomy.

Nielsen, R. L. 1995. Planting speed effects on stand establishment and grain yield of corn. *J. Prod. Agric.* 8(3): 391-393.

Plattner, C. E., and J. W. Hummel. 1996. Corn plant population sensor for precision agriculture. In *Proc. 3rd Intl. Conference on Precision Agriculture,* 785-794. P. C. Robert, R. H. Rust, and W. E. Larson, eds. Madison, Wisc.: ASA-CSSA-SSSA.

Porter, P. M., D. R. Hicks, W. E. Lueschen, J. H. Ford, D. D. Warnes, and T. R. Hoverstad. 1997. Corn response to row width and plant population in the northern Corn Belt. *J. Prod. Agric.* 10(2): 293-300.

Shrestha, D. S., and B. L. Steward. 2003. Automatic corn plant population measurement using machine vision. *Trans. ASAE* 46(2): 559-565.

Shrestha, D. S., and B. L. Steward. 2005. Shape and size analysis of corn plant canopies for plant population and spacing sensing. *Applied Eng. in Agric.* 21(2): 295-303.

Shrestha, D. S., B. L. Steward, and S. J. Birrell. 2004a. Video processing for early stage maize plant detection. *Biosystems Eng.* 89(2): 119-129.

Shrestha, D. S., B. L. Steward, K. R. Thorp, and B. Li. 2004b. A rapid video frame correspondence algorithm for agricultural video field surveying. ASAE Paper No. 043058. St. Joseph, Mich.: ASAE.

Smith, G. M., and E. J. Milton. 1999. The use of the empirical line method to calibrate remotely sensed data to reflectance. *Intl. J. Remote Sensing* 20(13): 2653-2662.

Thenkabail, P. S., R. B. Smith, and E. DePauw. 2000. Hyperspectral vegetation indices and their relationships with agricultural crop characteristics. *Remote Sensing Environ.* 71(2): 58-182.

Thorp, K. ., L. Tian, H. Yao, and L. Tang. 2004. Narrow-band and derivative-based vegetation indices for hyperspectral data. *Trans. ASAE* 47(1): 291-299.

Wanjura, D. F., D. R. Upchurch, S. J. Maas, and J. C. Winslow. 2003. Spectral detection of emergence in corn and cotton. *Precision Agric.* 4(4): 385-399.

Widdicombe, W. D., and K. D. Thelen. 2002. Row width and plant density effects on corn grain production in the northern Corn Belt. *Agron. J.* 94(5): 1020-1023.

Vanderlip, R. L., J. C. Okonkwo, and J. A. Schaffer. 1988. Corn response to precision of within-row plant spacing. *Applied Agric. Res.* 3(2): 116-119.

Yao, H., and L. Tian. 2004. Practical methods for geometric distortion correction of aerial hyperspectral imagery. *Applied Eng. in Agric.* 20(3): 367-375.